Interpretation®

Subsurface fluid flow focused by buried volcanic complexes in sedimentary basins

Journal:	*Interpretation*
Manuscript ID	INT-2016-0205.R1
Manuscript Type:	2015-12 Subsurface expression of igneous systems and their impacts on petroleum systems
Date Submitted by the Author:	n/a
Complete List of Authors:	Holford, Simon; The University of Adelaide, The Australian School of Petroleum Schofield, Nick; Geology and Petroleum Geology Reynolds, Peter; University of Adelaide, Australian School of Petroleum
Keywords:	Australia, volcanics, 3D, fluid, imaging
Subject Areas:	Case studies, Structural, stratigraphic, and sedimentologic interpretation

Subsurface fluid flow focused by buried volcanoes in sedimentary basins: evidence from 3D seismic data, Bass Basin, offshore southeastern Australia

Simon P. Holford[1,], Nick Schofield[2], and Peter Reynolds[1]

[1]Australian School of Petroleum, University of Adelaide, SA 5005, Australia

(simon.holford@adelaide.edu.au; peter.reynolds@adelaide.edu.au)

[2]Department of Geology and Petroleum Geology, University of Aberdeen, AB24 3UE, UK

(n.schofield@abdn.ac.uk)

Abstract

There is growing evidence that intrusive magmatic bodies such as sills and dikes can influence the migration of fluids in the deep subsurface. This influence is largely due to permeability contrasts with surrounding sedimentary rocks or because of interconnected open fractures within and around intrusions acting as conduits for migrating fluids. The role of buried volcanoes in influencing cross-stratal fluid migration in sedimentary basins is less well established. However, several studies have highlighted spatial linkages between extinct hydrothermal vent complexes and fluid seepage, suggesting buried extrusive features can also influence subsurface fluid flow pathways, potentially leading to migration of hydrocarbon fluids between source and reservoir. Here we present 3D seismic reflection data from the Bass Basin in offshore southeastern Australia that images an early Miocene volcanic complex with exceptional clarity. This volcanic complex is now buried by <1.3 km of younger sediments. The largest volcano within this complex is directly overlain by a vertical feature interpreted to be a fluid escape pipe, which extends vertically for ~700 m across the late Miocene-Pliocene succession. We suggest the buried volcanic complex was able to focus vertical fluid migration to the base of the pipe because its bulk permeability was higher than that of the overlying claystone sequence. The fluid escape pipe may have initiated through either: 1) hydraulic fracturing following fluid expulsion from a deep, overpressured sub-volcanic source region; 2) differential compaction and doming of the overlying claystones; or 3) through a combination of these processes. Our results suggest a hitherto

unrecognized role for buried volcanoes in influencing dynamic subsurface processes in sedimentary basins. In particular, our study highlights that buried volcanoes may facilitate cross-stratal migration of hydrocarbons from source to reservoir, or through sealing horizons.

Introduction

Volcanic and intrusive igneous rocks are found in many types of sedimentary basins, and are particularly common in basins that form due to lithospheric stretching i.e. rift and passive margin basins (e.g. Planke et al, 2000; White et al., 2003; Holford et al, 2012; Magee et al., 2016). Buried volcanic sequences and shallow intrusive complexes where magma stalled several kilometers below the paleolandsurface are thus frequently encountered during petroleum exploration and production. A number of studies have sought to identify the impact of this magmatism on the elements and processes of the petroleum system (e.g. Schutter, 2003; Planke et al., 2005; Rohrman, 2007; Holford et al., 2012, 2013; Rateau et al., 2013; Millett et al., 2016; Schofield et al., 2016).

A particular focus of previous work has been to assess the influence of intrusive igneous bodies on subsurface fluid migration. Mafic sills and laccoliths can generate focused subsurface fluid flow through the high flux of hydrothermal fluids derived from the magma by devolitization, and from host sediments by conductive heating and thermal pumping of pore fluids (Delaney, 1987; Einsele, 1992; Cartwright et al., 2007). This flux often leads to the formation of hydrothermal pipes, which typically emanate from the inclined lateral margins of sills or from ridge-like junctions within sills, and which exhibit a considerable range of diameter (~0.1 to 3 km) and height (up to 2.5 km) (Svensen et al., 2004; Hansen, 2006; Cartwright et al., 2007). Several recent studies have proposed that igneous intrusions can also influence the post-emplacement migration pathways of other basinal fluids, including hydrocarbons, over long timescales (Holford et al., 2013; Rateau et al., 2013; Schofield et al., 2015, 2016). Based on a detailed analysis of wells that penetrate intrusions in the Faroe Shetland Basin, Rateau et al. (2013) suggest that some low-permeability intrusions (and/or the surrounding contact metamorphic zones) have created barriers to fluid flow, whilst some intrusions may have acted as fractured conduits to migrating gas. Schofield et al.

(2015) demonstrate a compelling spatial relationship between the Tormore gas field and underlying sills, and proposed that fractured intrusions may have provided a preferential migration pathway through otherwise impermeable Paleocene shales.

Though basaltic lava flows can act as productive aquifers (e.g. within the Columbia River Group in the NW United States; Fetter, 2001), the influence of buried volcanoes on subsurface hydrocarbon migration is less well understood. The primary and secondary porosity and permeability of volcanic rocks can vary widely (Schutter, 2003; Millett et al., 2016), and there are numerous instances of both pyroclastic rocks and lavas acting as either reservoirs or seals (Schutter, 2003; Holford et al., 2012), thus acting as end-points to migration pathways. Noteworthy examples include the Jatibarang Field in Java where >1.2 billion barrels of oil and >2.7 TCF of gas have been produced from fractured, late Eocene-early Oligocene andesitic tuffs (Kartanegara at el., 1996), and the Kipper Field in the Gippsland Basin, Australia where a 328 m gross gas column is top sealed by >100 m of altered Campanian basalts (Sloan et al., 1992).

However, there are comparatively few reported occurrences of buried volcanoes influencing focused subsurface fluid flow over long timescales. This is somewhat surprising because buried and relatively pristine volcanoes, are common within the oceanic domain (e.g. seamounts and off-ridge axis vents; Mottl et al., 1998) and are being increasingly identified along continental margins (e.g. Holtar and Forsberg, 2000; Jackson, 2012; Magee et al., 2013, 2015; Reynolds et al., 2017). The burial of extrusive sequences by post-eruption sediments can potentially result in profound permeability contrasts and therefore enhance the potential for focused subsurface fluid flow, as indicated by a number of intriguing case studies by Svensen et al. (2003, 2006, 2008). For example, Svensen et al. (2003) describe a ~50-million-year record of seep carbonate growth within Eocene-Pliocene sediments above an extinct sill-fed hydrothermal vent complex of Paleocene age in the Vøring Basin. Their analysis indicated that the hydrothermal vent complex acted as a long-lived, high permeability zone during burial of the basin.

The principal aim of this paper is to understand the relationship between buried volcanoes and focused cross-stratal fluid flow in sedimentary basins. We use three-dimensional (3D) seismic reflection data from the Bass Basin, offshore southeastern Australia (Fig. 1). This is an excellent location to address this aim because it contains multiple, well-imaged volcanic features that have been penetrated by drilling and are interpreted to be monogenetic pillow volcanoes and tuff cones, rather than hydrothermal vent complexes (Reynolds et al., 2017). Here we focus on an intriguing spatial linkage whereby the post-eruption sediments within the Yolla 3D seismic survey host a feature interpreted to be a fluid escape pipe, which directly overlies a monogenetic tuff cone. We explore how the buried volcano may have controlled fluid migration over a timescale of ~20 Myr since the cessation of eruptive activity. We also discuss the broader implications of fluid migration focused by buried volcanic complexes in sedimentary basins.

Geological Setting

The Bass Basin is an intracratonic rift basin located offshore between Victoria and northern Tasmania, southern Australia (Fig. 1). Active extensional deformation related to lithospheric stretching in the Southern Ocean and Tasman Sea culminated in the mid-Eocene, resulting in the formation of a number of NW-SE trending half-grabens including the Yolla Trough (Holford et al., 2012). Many petroleum exploration wells have penetrated intrusive and volcanic rocks of Cretaceous-Miocene age in this basin, with peaks in magmatic activity observed during the Paleocene (i.e. syn-rift) and Oligocene-Miocene (i.e. post-rift; Holford et al., 2012; Meeuws et al., 2016; Reynolds et al., 2017). The igneous rocks that have been encountered by drilling are generally mafic, consistent with the broader record of extensive late Cenozoic basaltic volcanism in northwestern Tasmania and in the Newer Volcanics Province, to the north of the Bass Basin (Holt et al., 2013; Meeuws et al., 2016).

The Yolla-1 well was drilled in 1985 resulting in the discovery of the Yolla gas field (Lennon et al., 1999). A ~20 Ma volcaniclastic sequence was encountered at depths between 1237-

1305 m (Fig. 2), comprising highly altered volcanic tuff, with abundant alteration to clays and calcite, interbedded with sandstones, claystones and siltstones (Wheeler and Kjellgren, 1986). The sandstones contained fragments of mafic rock (Boral Energy, 1998). This volcaniclastic sequence is overlain by a ~500 m thick sequence of early Miocene marine calcareous claystones deposited in water depths of between 90-140 m (Boral Energy, 1998). This volcaniclastic sequence is clearly visible on the regional seismic profile presented in Fig. 3. Other igneous rocks encountered by the Yolla-1 well include a medium to fine-grained gabbroic intrusion dated as latest Oligocene by K-Ar and a sequence of highly altered basalts of probable late Cretaceous-early Paleocene age were encountered in deeper sections of the well (Wheeler and Kjellgren, 1986). The Bass-1 well, drilled ~10 km to the NW of Yolla-1 penetrated a younger (~16 Ma) volcano that is also visible on Fig. 3 (Holford et al., 2012; Reynolds et al., 2017). The Tilana-1 well, drilled ~16 km to the SE, penetrated ~150 m of vesicular basalts at a similar stratigraphic level to the volcaniclastic sequence in Yolla-1, whilst $^{40}Ar/^{39}Ar$ dating of a gabbroic intrusion between 2172-2193 m yielded an early Miocene age (Blevin and Cathro, 2008).

Reynolds et al. (2017) have recently conducted a detailed study of Miocene volcanism in the Bass Basin, using the Yolla 3D and Labatt 3D seismic reflection surveys. They identified three separate phases of volcanic mound construction occurring between approximately 20 and 16 Ma. The ~20 Ma volcanism corresponds to that observed within the Yolla 3D survey, and the 16 Ma volcanism corresponds to that drilled by Bass-1. On the basis of seismic reflection characteristics supplemented by well data, Reynolds et al. (2017) interpreted the mounds to be monogenetic volcanoes composed of hyaloclastite and/or pyroclasts.

Data and methods

The Yolla 3D seismic reflection survey was acquired in 1994 and covers 260 km^2 with 12.5 x 25 m bin spacing. The seismic data is pre-stack time migrated and is displayed with SEG Normal Polarity. The dominant frequency at Miocene levels is 40-50 Hz, and the frequency range is 5-125

Hz. At an interval velocity of 3000 m s^{-1} (based on Yolla-1 well data) this results in a vertical resolution of 15-19 meters.

We mapped five seismic horizons within the study area. The ages of these horizons were constrained by synthetic seismograms that enabled them to be tied to stratigraphic information from the Yolla-1 and Bass-1 wells. Further details on the well-seismic ties are provided in Reynolds et al. (2017). The Mid Miocene and Lower Mid Miocene horizons occur above the volcano penetrated by Yolla-1, which occurs within a package bound by the Top Volcanic and Base Volcanic horizons. These horizons correspond to the TV3 and BV3 horizons in Reynolds et al. (2017). The Eastern View Coal Measures horizon occurs below the volcanic package.

To assist our interpretation and help visualize volcanic and related features we computed a coherency cube from the original reflection volume. We also generated a spectral decomposition volume (Henderson et al., 2007), with a blend involving frequencies red = 27 Hz, green = 33 Hz and blue = 57 Hz found to highlight supra-volcanic features clearly.

Interpretation of 3D seismic data

Volcanic features

A representative inline from the 3D survey is shown in Fig. 4A. The TV horizon is marked by a laterally discontinuous bright reflection. This horizon forms the highest amplitude event after the seabed reflection due to the acoustic impedance contrast with the overlying claystones. The TV horizon defines a mound-like structure with maximum dips of 15–20° that culminates at ~0.85 s TWT (~0.2 s above its regional elevation), 2 km NE of the well location (Fig. 4A). An amplitude time slice at ~1 s TWT shows that the mound comprised of several, partially overlapping smaller mounds (V1-V3) that possess circular to elliptical planform geometries (Fig. 5A). A separate series of smaller mounds aligned in an N-S orientation occur NW of Yolla-1 (V4-V6). The largest identifiable mound, which is closest to Yolla-1 (V1), has a diameter of ~3 km at 1 s TWT.

The diameter, height and volume of the mounds, and their seismic reflection facies are consistent with basaltic tuff cones (Reynolds et al., 2017). We hereafter refer to this as the Yolla volcanic complex, which comprises three overlapping volcanoes (V1-V3). Similar tuff cones of late Oligocene age occur onshore at Airey's Inlet (Cas et al., 1993), 215 km NW of Yolla-1 (Fig. 1). We infer that the tuff cone was emplaced in a shallow marine environment, similar to pristine submarine Eocene volcanoes in the Ceduna sub-basin described by Jackson (2012). Sedimentological and palynological data from the overlying calcareous claystones at Yolla-1 indicates deposition of these rocks in water depths of >90 to 140 meters of water, with calcareous sediments winnowed off a nearby bryozoan bank with associated clay flux (Boral Energy, 1998). The construction of the volcano in a shallow marine environment would have resulted in rapid alteration of the volcaniclastic deposits (c.f. Kano, 1998), consistent with the highly altered nature of the volcanic rocks encountered by Yolla-1.

Sub-volcanic features

An array of sub-linear, near-vertical, ~N-S trending zones of seismic disturbance (Fig. 3A,B), occurs at >1 s TWT (Fig. 4A). In map view these zones are can be distinguished from faults on the basis of their orientation, cross-cutting relationships and the fact that there is no evidence for vertically offset reflections across them (Fig. 4A). The maximum width of these zones is ~100 m, and lengths vary between 2 to >15 km. There is strong alignment between the ~N-S orientations of these zones and the volcanoes (Fig. 5B). We do not interpret these zones to be sub-volcanic artefacts, because they are not restricted to occurring just beneath the volcanoes (Fig. 5B). We instead interpret them to be near-vertical dikes, which supplied magma to the overlying volcanoes. Though a number of small sills have been intersected by wells in the Bass Basin (e.g. Yolla-1, Tilana-1; Holford et al., 2012; Meeuws et al., 2016), and sills are present in the Labatt 3D survey situated NW of the Yolla survey (Reynolds et al., 2017), we find no clear evidence for large, seismically-resolvable sills located beneath the Yolla volcanic complex.

Supra-volcanic features

The Yolla volcanic complex is overlain by a sequence of calcareous claystones that reaches ~400 m in thickness SW of Yolla-1, and which contains a conspicuous polygonal fault system (PFS) (Figs. 3, 4A, 5E). The LMM horizon, which is a prominent reflection event (LMM) of lower mid-Miocene age (~16 Ma) that bounds the top of this package, is gently folded over the volcanic complex. A prominent dome is situated above V1, and divergent reflections are observed within this claystone package. These observations are suggestive of differential compaction of the claystone package, which thins by up to 40% above the volcanic complex. The flanking claystones would compact more and at shallower burial depths than across the adjacent volcano.

Mapping of LMM reveals several amplitude anomalies that overlie the volcanic complex. These anomalies are well imaged using spectral decomposition, which can reveal subtle frequency response characteristics. An RGB blend displayed on LMM shows a subcircular feature (labelled feature A; diameter ~1 km), which is domal in cross-section and directly overlies the largest vent (V1) of the volcanic complex (Fig. 5C). Several frequency anomalies occur around the subcircular feature, the largest of which (labelled feature B) occurs to the NE and covers an area of ~13 km^2. These features have lower seismic amplitude than the TV reflection (Fig. 4), and we do not interpret them to be volcanic in origin. The frequency response is also not consistent with these features being volcanic, as volcanic rocks tend to produce responses from across the frequency spectrum. We are uncertain as to what is driving the frequency response, other than a contrast in lithological properties and/or fluid content.

The shallow (<0.7 s TWT) section above the LMM horizon is characterized by parallel, unfaulted strata, corresponding to a sequence of mid-Miocene-Recent shallow marine calcarenites (Wheeler and Kjellgren, 1986). A ~700 m high, near-vertical zone of disrupted reflections forming a pipe-like structure is developed directly over both the mid-Miocene dome (A), the largest vent within the volcanic complex and the zone of discontinuous reflections linking the two (V1; Fig. 4C). A series of amplitude time slices through the mid-Miocene-Recent section confirm this spatial

207 alignment and show that this structure possesses a circular planform (maximum diameter ~625 m)
208 and extends to just beneath the sea floor (Fig. 5E).

209

210 Discussion

211 We have described a pristine early Miocene (~20 Ma) volcanic complex buried within the
212 post-rift succession of a sedimentary basin offshore southeastern Australia. An unusual finding is
213 that both a series of amplitude and frequency anomalies and a ~700 m high, sub-vertical pipe-like
214 structure directly overlie the main volcano within the complex.

215 *Relationship between buried volcanic complex and supra-volcanic features*

216 We first present two alternative interpretations for the anomalies that are observed from
217 mapping of the LMM horizon. One interpretation is that they are related to differential compaction
218 of the claystone sequence, because the lateral extent of feature B broadly corresponds to the
219 topography of the underlying volcanic complex. The second interpretation is that feature B is a
220 sedimentary density current deposit extending away from a source sedimentary volcano, which here
221 is expressed as a subcircular frequency anomaly (feature A). In cross section the sequence beneath
222 the conduit is characterised by a pipe-like zone of discontinuous reflections (Fig. 4B), and in
223 combination, these features are reminiscent of analogous structures within fine-grained calcareous
224 sediments in the North Sea interpreted to be mud volcanoes (Andresen et al., 2010). Based on the
225 spatial correspondence between the frequency anomalies and the underlying topography of the
226 individual volcanoes within the complex, we consider that an origin related to differential
227 compaction is most likely. However, we cannot discount the possibility that features A and B
228 represent a sediment volcano and sedimentary density current deposit, respectively.

229 We interpret the supra-volcanic, pipe-like structure to be a fluid-escape pipe (Fig. 6C).
230 Similar structures are recognized on 3D seismic data from many continental margin basins (e.g.
231 Ligtenberg, 2005; Cartwright et al., 2007; Moss and Cartwright, 2010). Many of these structures are
232 thought to represent natural hydraulic fractures that form following critical pressurization of

subsurface aquifers and hydrocarbon reservoirs, enabling fluid escape (Moss and Cartwright, 2010), though other potential mechanisms for pipe genesis include erosive fluidization and capillary invasion (Cartwright and Santamarina, 2015).

We speculate that the supra-volcanic pipe that extends towards the seabed formed geologically recently, when highly pressured fluids and/or gases originating from deeper parts of the basin migrated upwards and were focused by the Yolla volcanic complex. Basin modeling indicates that the late Paleocene-early Eocene-age coals, thought to have sourced the nearby Yolla gas accumulation, began to expel hydrocarbons at ~5 Ma (Arian et al., 2010). Furthermore, significant overpressures occur at depths >2.7 km in the Bass Basin, coincident with the depth of the oil expulsion window (Arian et al., 2010).

The integrity of the seal above the reservoir that hosts the proximal Yolla gas field is uncompromised, implying significant compartmentalization of fluid flow and pressure regimes at depths >1.5 km, possibly aided by the network of subvolcanic dikes. We suggest that fluids and/or gases from mature source rocks to the east of the fault-bounded Yolla closure migrated upwards to the base of the claystone sequence, which we infer has low-permeability, and were then focused by the volcanic complex, which formed a structurally-high pressure foci (c.f. Sun et al., 2012; Cartwright and Santamarina, 2015). Fluids may have been preferentially exploited and focused by internal fractures and high permeability pathways within the volcanic complex, or along its margins by lateral pressure transfer. Because there is no core from the Torquay Group, we are unable to directly constrain the permeability of the claystones or the volcanic rocks.

The pipe itself may have formed due to hydraulic fracturing following fluid expulsion from a deep, overpressured sub-volcanic source region, or due to differential compaction of the overburden of the Yolla volcanic complex, which is most pronounced over the largest volcano (V1). We cannot discriminate between these scenarios, but in both cases we infer that the volcanic complex has acted to focus fluids to the base of the pipe.

An alternative explanation for the supra-volcanic fluid escape pipe is that it formed due to the dewatering or reactivation of the polygonally-faulted claystone sequence. A number of studies have identified spatial associations between pockmarks or fluid escape pipes and polygonal faults (Berndt et al., 2003; Gay and Berndt, 2007; Tewkesbury et al., 2014). Gay and Berndt (2007) present a case study from the Vøring Basin, Norwegian Margin, where the genesis of a PFS within the late Pleistocene Naust Formation prompted the reactivation of an inactive PFS within the deeper, upper Miocene-lower Pliocene Kai Formation. The interconnectivity between these tiered PFSs permitted upward migration of fluids, resulting in a range of pipes and seabed pockmarks. However, we note that Cartwright (2014) points out that there are many examples of PFSs where there is no association with fluid escape pipes.

Although we consider the above hypothesis plausible, our preferred hypothesis is that the location of the fluid escape pipe has been directly controlled by the deeper volcanic complex. Critically, we note that the seismic data shows evidence for disrupted reflectors between the TV and LMM horizons, directly above V1 (Fig. 4C, Fig. 5E). This suggests that the base of the fluid escape pipe is directly linked to the volcanic complex, which acted as a structurally-high pressure foci. Furthermore, whilst other regions that potentially show associations between PFSs and fluid escape typically contain multiple pipes, the only clear fluid escape pipe within the seismic survey is that which is located directly above V1. Because the supra-volcanic pipe almost extends to the seabed, it is likely to have formed geologically recently, which rules out a link to dewatering of the PFS-hosting claystones during early burial, though it is plausible that the PFS may have retained fluids during burial and released these through the pipe during later seepage. It is also possible that the pipe may have formed through a combination of the genetic processes above. Whatever the origin of the pipe, it does not appear to be sustaining an active fluid flow system, as geochemical surveying over the Yolla gas field conducted in 1989 found no evidence for seepage of hydrocarbons at this location (O’Brien et al., 1992).

284 ***Model accounting for spatial linkages between buried volcanic complex and focused fluid flow***

285 Here we advance our preferred three-stage model to account for the spatial linkage between 286 the Yolla volcanic complex and the supra-volcanic fluid expulsion pipe. Stage one involves the 287 development of the Yolla volcanic complex at ~20 Ma, as a result of the eruption of basaltic magma 288 in a shallow marine setting (Fig. 6A). The complex comprises a number of partially overlapping 289 volcanoes, and we infer that these were fed via N-S trending dikes (Fig. 5B).

290 The next stage involves the burial beneath a package of calcareous claystones (Fig. 6B), 291 which likely protected the Yolla volcanic complex from large-scale degradation by post-eruption 292 erosion. This claystone package contains an extensive polygonal fault system (PFS), which 293 presumably developed early burial (c.f. Cartwright, 2011). The frequency anomalies observed at the 294 top of this sequence (on the LMM horizon) probably represent differential compaction structures, 295 though we cannot discount the possibility that these formed because of sediment expulsion from a 296 mud volcano; this would imply that the volcanic complex has repeatedly modulated subsurface 297 fluid and sediment recycling.

298 The third and final stage of our model pertains to the genesis of the supra-volcanic pipe 299 overlying V1. We hypothesize that the regionally extensive sequence of fine-grained lower 300 Miocene claystones acted as a low-permeability sealing sequence, forming a barrier to the vertical 301 migration of pressured fluids and/or gases expelled from sub-volcanic source rocks. Migrating 302 fluids were subsequently focused by the volcanic complex, which acted as a structurally-high 303 pressure foci.

304 ***Implications for fluid flow focused by buried volcanoes***

305 Our preferred model for fluid flow focused by an extinct volcanic complex is analogous that 306 proposed by Svensen et al. (2003) to explain the presence of seep carbonates in Eocene-Pliocene 307 strata above a late Paleocene age hydrothermal vent complex in the Vøring Basin. Svensen et al. 308 (2003) argued that hydrocarbons from deeper in the basin migrated towards and through the

hydrothermal vent complex and underlying zone of brecciation, which acted as a zone of high vertical-permeability, focussing fluid migration during basin subsidence.

Though the early Miocene volcanic section drilled by Yolla-1 comprises altered pyroclastic deposits, based on detailed seismic mapping of numerous volcanoes of similar age in the Bass Basin, (Reynolds et al., 2017), we think it likely that the composition of the volcanoes within the Yolla volcanic complex includes basaltic hyaloclastite and tuff, similar to the late Oligocene Airey's Inlet Volcanic Complex, to the NW of our study area (Cas et al., 1993). Porosity and permeability within volcanic rocks can be highly variable, and is dependent on a wide range of syn and post-eruption processes (Millett et al., 2016). Whilst individual units of highly vesicular basalts and unaltered hyaloclastite may have high permeabilities (i.e. $>10^{-12}$ m^2) (Millett et al., 2016), facies variations and internal heterogeneities within layered volcanic sequences (Planke, 1994; Archer et al., 2005) suggest that the potential for bulk vertical permeability in an undeformed volcanic pile is low. However, volcanoes such as those within the Yolla volcanic complex typically include many sub-vertical pipes, fractures and faults (e.g. Sohn and Chough, 1992). If such pipes, fractures and faults are not mineralized, they could enhance vertical permeability. Fracturing at the margins of sub-vertical dikes within the volcanic complex may also provide pathways for fluid flow (Senger et al., 2015).

The precise mechanisms of fluid migration through buried volcanoes remains uncertain, and may require targeted scientific drilling (e.g. through IODP or ICDP) to obtain high quality data on the permeability, internal architecture and diagenetic state of buried volcanoes, in relation to the fluid flow properties of surrounding sedimentary sequences. However, given that buried volcanoes are being increasingly recognised within sedimentary successions at continental margins, focused fluid migration associated with 'leaky' volcanoes may be more common than presently assumed. Several recent studies have argued that fractured sub-volcanic sills can provide conduits for fluid migration (Rateau et al., 2013; Schofield et al., 2015). The highest potential for subsurface fluid flow through volcanoes may therefore be associated with sill-fed volcanoes (e.g. Jackson, 2012; Magee et al., 2013, 2016).

Conclusions

1. Buried volcanoes, which are common features in continental margin basins, can potentially influence subsurface fluid flow over long timescales after their extinction.
2. Earlier studies have identified links between igneous intrusions, hydrothermal vent complexes and long-term fluid migration, yet we are unaware of any prior demonstrations of subsurface fluid flow focused by buried volcanoes using 3D seismic data.
3. The volcanic complex located offshore southern Australia described in this study was presumably able to directly focus the vertical migration of fluids because its bulk permeability was higher than that of the overlying polygonally-faulted claystone sequence.
4. Our results imply that buried volcanic complexes may play a hitherto underappreciated role in dynamic processes in sedimentary basins by modulating subsurface fluid and pressure regimes.
5. There is growing evidence that sub-volcanic igneous intrusions can influence the post-emplacement migration pathways hydrocarbons, and our findings suggest that buried volcanoes may also play an important role in assisting the cross-stratal migration of hydrocarbons from source to reservoir, or through sealing horizons.

Acknowledgments

We acknowledge funding from ARC Discovery Projects DP0897612 and DP1601158, and IHS and ffA for provision of software. We thank Sverre Planke, Chris Jackson, Qiliang Sun, Joe Cartwright, Gerome Calves, Henrik Svensen and Mads Huuse for helpful and constructive reviews of this manuscript. We also thank Chris Jackson for editorial assistance. This contribution represents TRaX #XXX.

References

Archer, S. G., S. C. Bergman, J. Iliffe, C. M. Murphy, and M. Thornton, 2005, Palaeogene igneous rocks reveal new insight into the geodynamic evolution and petroleum potential of the Rockall Trough, NE Atlantic Margin: Basin Research, **17,** 171-201.

Arian. N., P. Tingate, R. R. Hillis and G. W. O'Brien, 2010, Petroleum systems of the Bass Basin: A 3D modeling perspective: APPEA Journal, **50,** 511-534.

Andresen, K. J., O.R. Clausen and R. B. Jørgensen, 2010, A composite mud volcano system in the Chalk Group of the North Sea Central Graben: Journal of the Geological Society, **167,** 1209-1224.

Berndt, C., S. Bünz and J. Mienert, 2003, Polygonal fault systems on the mid-Norwegian margin: a long-term source for fluid flow: Geological Society of London, Special Publications, **216,** 283-290.

Blevin, J. E. and D. L. Cathro, 2008, Australian Southern Margin Synthesis, Project GA707: Client report to Geoscienec Australia by FrOG Tech Pty Ltd.

Blevin, J. E., K. R. Trigg, A. D. Partridge, C. J. Boreham and S. C. Lang, 2005, Tectonostratigraphy and potential source rocks of the Bass Basin: APPEA Journal, **45,** 601-621.

Boral Energy, 1998, Yolla 2 Well Proposal T/RL1.

Cartwright, J., 2011, Diagenetically induced shear failure of fine-grained sediments and the development of polygonal fault systems: Marine and Petroleum Geology, **28,** 1593-1610.

Cartwright, J., 2014. Are outcrop studies the key to understanding the origins of polygonal fault systems? Geology, **42,** 559-560.

Cartwright, J., M. Huuse, and A. Aplin, 2007, Seal bypass systems: AAPG Bulletin, **91,** 1141-1166.

Cummings, A. M., R. R. Hillis and P. R. Tingate, 2004, New perspectives on the structural evolution of the Bass Basin: implications for petroleum prospectivity: PESA Special Publications, 133-149.

Cas, R., C. Simpson. and H. Sato, 1993, Newer volcanics province: Processes and products of phreatomagmatic activity: Geoscience Australia Record 1993/64.

Delaney, P. T., 1987, Heat transfer during the emplacement and cooling of dykes: Geological Association of Canada, Special Paper, **34,** 31-46.

Einsele, G., 1992, Sedimentary basins, evolution, facies and sediment budget: Berlin, Springer-Verlag, 628 p.

Fetter, C. W., 2001, Applied hydrogeology (fourth edition): New Jersey, Prentice-Hall, 599 p.

Gay, A. and C. Berndt, 2007, Cessation/reactivation of polygonal faulting and effects on fluid flow in the Vøring Basin, Norwegian Margin: Journal of the Geological Society, **164,** 129-141.

Grove, C., 2013. Submarine hydrothermal vent complexes in the Faroe-Shetland basin: insights from 3D seismic and petrographical data. Geology 41, 71-74.

Hansen, D. M., 2006, The morphology of intrusion-related vent structures and their implications for constraining the timing of intrusive events along the NE Atlantic margin: Journal of the Geological Society, **163,** 789-800.

Henderson, J., S. J. Purves, and C. Leppard, 2007, Automated delineation of geological elements from 3D seismic data through analysis of multi-channel, volumetric spectral decomposition data: First Break, **25,** 87-93.

Holford, S. P., N. Schofield, J. D. MacDonald, I. R. Duddy and P. F. Green, 2012, Seismic analysis of igneous systems in sedimentary basins and their impacts on hydrocarbon prospectivity: examples from the southern Australian margin: APPEA Journal, **52,** 229-252.

Holford, S. P., N. Schofield, C. A.-L. Jackson, C. Magee, P. F. Green and I. R. Duddy, 2013, Impacts of igneous intrusions on source and reservoir potential in prospective sedimentary basins along the western Australian continental margin: West Australian Basins Symposium, 18–21 August 2013.

Holford, S. P., A. K. Tuitt, R. R. Hillis, P. F. Green, M. S. Stoker, I. R. Duddy, M. Sandiford and D. R. Tassone, 2014, Cenozoic deformation in the Otway Basin, southern Australian margin: implications for the origin and nature of post-breakup compression at rifted margins: Basin Research, **26,** 10-37.

Holtar, E. and A. W. Forsberg, 2000; Postrift development of the Walvis Basin, Namibia: results from the exploration campaign in Quadrant 1911: AAPG Memoirs, **73,** 429-446.

Jackson, C. A.-L., 2012, Seismic reflection imaging and controls on the preservation of ancient sill-fed magmatic vents: Journal of the Geological Society, **169,** 503-506

Kano, K., 1998, A shallow-marine alkali-basalt tuff cone in the Middle Miocene Jinzai, Formation, Izumo, SW Japan: Journal of Volcanology and Geothermal Research, **87,** 173-191.

Kartanegara, A.L., R. N. Baik and M. A. Ibrahim, 1996, Volcanics oil bearing in Indonesia: AAPG 1996 Annual Convention, Meeting Abstracts, **5,** A73.

Ligtenberg, J. H., 2005, Detection of fluid migration pathways in seismic data: implications for fault seal analysis: Basin Research, **17,** 141-153.

Lennon, R. G., R. J. Suttill, D. A. Guthrie, and A. R. Waldron, 1999, The renewed search for oil and gas in the Bass Basin: results of Yolla-2 and White Ibis-1: APPEA Journal, **37,** 248-262.

Magee, C., E. Hunt-Stewart, and C. A.-L. Jackson, 2013, Volcano growth mechanisms and the role of sub-volcanic intrusions: insights from 2D seismic reflection data: Earth and Planetary Science Letters, **373,** 41–53.

Magee, C., O. B. Duffy, K. Purnell, R. E. Bell, C. A.-L. Jackson and M. T. Reeve, 2015, Fault-controlled fluid flow inferred from hydrothermal vents imaged in 3D seismic reflection data, offshore NW Australia: Basin Research, **28,** 299-318.

Magee, C., J. D. Muirhead, A. Karvelas, S. P. Holford, C. A.-L. Jackson, I. D. Bastow, N. Schofield, C. T. E. Stevenson, C. McLean, W. McCarthy and O. Shtukert, 2016, Lateral magma flow in mafic sill complexes: Geosphere, **12,** 809-841.

Meeuws, F. J. E., S. P. Holford, J. D. Foden and N. Schofield, 2016, Distribution, chronology and causes of Cretaceous-Cenozoic magmatism along the magma-poor rifted southern Australian margin: Links between mantle melting and basin formation: Marine and Petroleum Geology, **73,** 271-298.

Millett, J. M., A. D. Wilkins, E. Campbell, M. J. Hole, R. A. Taylor, D. Healy. D. A. Jerram, D. W. Jolley, S. Planke, S. G. Archer and A. Blischke, 2016, The geology of offshore drilling through basalt sequences: Understanding operational complications to improve efficiency: Marine and Petroleum Geology, **78,** 1177-1192.

Moss, J. L. and J. Cartwright, 2010, 3D seismic expression of km-scale fluid escape pipes from offshore Namibia: Basin Research, **22,** 481-501.

Mottl, M. J., G. Wheat, E. Baker, N. Becker, E. Davis, R. Feely, A. Grehan, D. Kadko, M. Lilley, G. Massoth, C. Moyer and F. Sansone, 1998, Warm springs discovered on 3.5 Ma oceanic crust, eastern flank of the Juan de Fuca Ridge: Geology, **26,** 51-54.

Planke, S., 1994, Geophysical response of flood basalts from analysis of wire line logs: Ocean Drilling Program Site 642, Vøring volcanic margin: Journal of Geophysical Research: Solid Earth, **99,** 9279-9296.

Planke, S., P. A. Symonds, E. Alvestad and J. Skogseid, 2000, Seismic volcanostratigraphy of large-volume basaltic extrusive complexes on rifted margins: Journal of Geophysical Research: Solid Earth, **105,** 19335-19351.

Planke, S., T. Rasmussen, S. S. Rey and R. Myklebust, 2005, Seismic characteristics and distribution of volcanic intrusions and hydrothermal vent complexes in the Vøring and Møre basins: Geological Society, London, Petroleum Geology Conference, **6,** 833-844.

Rateau, R., N. Schofield and M. Smith, 2013, The potential role of igneous intrusions on hydrocarbon migration, West of Shetland: Petroleum Geoscience, **19,** 259–272.

Reynolds, P., N. Schofield, R. J. Brown and S. Holford, 2017, The architecture of submarine monogenetic volcanoes - insights from 3D seismic data: Basin Research, 463 doi:10.1111/bre.12230.

464 Rohrman, M., 2007, Prospectivity of volcanic basins: Trap delineation and acreage delineation: AAPG Bulletin, **91,** 915-939.

466 Rollet, N., S. McGiveron, T. Hashimoto, R. Hackney, P. Petkovic, K. Higgins, E. Grosjean and G. A. Logan, 2012, Seafloor features and fluid migration in the Capel and Faust basins, offshore eastern Australia: Marine and Petroleum Geology, **35,** 269-291.

469 Schofield, N., S. Holford, J. Millett, D. Brown, D. Jolley, S. Passey, D. Muirhead, C. Grove, C., Magee, J. Murray, M. Hole, C. Jackson and C. Stevenson, 2015, Regional magma plumbing and emplacement mechanisms of the Faroe-Shetland Sill Complex: implications for magma transport and petroleum systems within sedimentary basins: Basin Research, doi:10.1111/bre.12164.

474 Schofield, N., D. A. Jerram, S. Holford, S. Archer, N. Mark, A. Hartley, J. Howell, S. Muirhead, P. Green, D. Hutton and C. Stevenson, 2016, Sills in sedimentary basins and petroleum systems: Advances in Volcanology, 10.1007/11157_2015_17.

477 Schutter, S. R, 2003, Hydrocarbon occurrence and exploration in and around igneous rocks: Geological Society of London, Special Publications, **214,** 7-33.

479 Senger, K., S. J. Buckley, L. Chevallier, Å. Fagereng, O. Galland, T. H. Kurz, K. Ogata, S. Planke and J. Tveranger, 2015, Fracturing of doleritic intrusions and associated contact zones: Implications for fluid flow in volcanic basins: Journal of African Earth Sciences, **102,** 70-85.

482 Sibson, R. H., 1995, Selective fault reactivation during basin inversion: potential for fluid redistribution through fault-valve action: Geological Society of London, Special Publications, **88,** 3-19.

485 Sloan, M. W., P. S. Moore and A. McCutcheon, 1992, Kipper – a unique gas discovery, Gipplsand Basin, Australia; APEA Journal, **35,** 1-8.

487 Sohn, Y. K. and S. K. Chough, 1992, The Ilchulbong tuff cone, Cheju Island, South Korea: Sedimentology, **39,** 523-544.

Sun, Q., S. Wu, J. Cartwright and D. Dong, 2012, Shallow gas and focused fluid flow systems in the Pearl River Mouth Basin, northern South China Sea: Marine Geology, **315-318,** 1-14.

Svensen, H., S. Planke, B. Jamtveit and T. Pedersen, 2003, Seep carbonate formation controlled by hydrothermal vent complexes: a case study from the Vøring Basin, the Norwegian Sea: Geo-Marine Letters, **23,** 351-358.

Svensen, H., S. Planke, A. Malthe-Sørensen, B. Jamviet, R. Myklebust, T. R. Eidem and S. S. Rey, 2004, Release of methane from a volcanic basin as a mechanism for initial Eocene global warming: Nature, **429,** 542-545.

Svensen, H., B. Ø. Jamtveit, S. Planke and L. Chevallier, 2006, Structure and evolution of hydrothermal vent complexes in the Karoo Basin, South Africa: Journal of the Geological Society, **163,** 671-682.

Svensen, H., G. Bebout, A. Kronz, L. Li, S. Planke, L. Chevallier and B. Jamtveit, 2008, Nitrogen geochemistry as a tracer of fluid flow in a hydrothermal vent complex in the Karoo Basin, South Africa: Geochimica et Cosmochimica Acta, **72,** 4929-4947.

Tewkesbury, B. J., J. P. Hogan, S. A. Kattenhorn, C. J. Mehrtens and E. A. Tarabees, 2014, Polygonal faults in chalk: Insights from extensive eposures of the Khoman Formation, Western Desert, Egypt: Geology, **42,** 479-482.

Wheeler, B.F. and R. M. Kjellgren, 1986, Yolla-1 final well report: Amoco Australian Petroleum Company.

White, N., M. Thompson and T. Barwise, 2003, Understanding the thermal evolution of deep-water continental margins: Nature, **426,** 334-343.

515

516 **Figure captions**

517 **Figure 1.** A: Location of Bass Basin, including approximate distribution of Cretaceous-
518 Cenozoic age igneous rocks, location of the Yolla 3D seismic survey and the regional seismic
519 profile shown in Figure 3. Inset map shows location of study area in relation to the Australian
520 continent. B: Summary chart of Bass Basin stratigraphy, depositional environments, tectonic
521 events, interpreted seismic horizons, and recorded episodes of extrusive and intrusive
522 magmatism. Modified after Cummings et al. (2014), timing of deformation modified after
523 Holford et al. (2014) and timing of magmatic events from Meeuws et al. (2016).

524 **Figure 2.** Lithologic, stratigraphic and sonic velocity and gamma ray log data for the shallowest
525 1600 m of rock section penetrated by the Yolla-1 well, showing the context of the interpreted
526 horizons within the Torquay Group.

527 **Figure 3.** A: Uninterpreted two-dimensional seismic reflection profile through the Bass and
528 Yolla volcanic complexes, highlighting multiple phases of Miocene volcanism. B: Interpreted
529 seismic profile, highlighting volcanoes (shaded in grey), sub-volcanic dikes (indicated by
530 dashed lines) and well penetrations of extrusive and intrusive igneous rocks. BV–Base of the
531 volcanic sequence penetrated by Yolla-1; EVCM–Top Eastern View Coal Measures (late
532 Eocene); LMM –Lower Mid-Miocene regional seismic marker; MM–Mid Miocene regional
533 seismic marker; PFS–Polygonal fault system bounded by LMM and TV; TV–Top volcanic
534 sequence.

535 **Figure 4**. A: Interpreted two-dimensional seismic inline 530 from the Yolla 3D survey tied to
536 the Yolla-1 well. Volcanoes 1, 2 and 3 of the Yolla volcanic complex are visible between 1.0-
537 1.2 s TWT, with V1 ca. 2 km to the NE of Yolla-1. A sub-vertical, supra-volcanic pipe occurs
538 between ca. 0.15-0.7 s TWT, directly above V1. BV–Interpreted base of the volcanic sequence
539 drilled by Yolla-1; EVCM–Top Eastern View Coal Measures (late Eocene); LMM –Lower Mid-
540 Miocene regional seismic marker; MM–Mid Miocene regional seismic marker; PFS–Polygonal

fault system; TV–Top volcanic sequence. B: Interpreted two-dimensional seismic crossline 1253 highlighting the folding of the LMM horizon directly above the largest volcano (V1) of the Yolla volcanic complex. C: Interpreted two-dimensional seismic inline 545 highlighting sub-vertical supra-volcanic pipe above V1. Location of these lines is shown in Fig. 5A.

Figure 5. A: Seismic amplitude time slice (1.052 s TWT). Volcanic sequences are marked by high amplitude events that are easily distinguishable from surrounding sedimentary rocks. Gas-water contact of the Yolla hydrocarbon field is projected upwards onto this slice. Six main volcanoes (V1-V6) and a number of smaller parasitic cones (PC) are identified. B: Seismic semblance time slice (1.880 s TWT), highlighting discontinuities within the seismic volume (shown in black). Slice is annotated to distinguish between generally curvilinear faults (shown by blue dashed lines), interpreted dikes (shown by red dashed lines) and the outlines of overlying volcanoes (orange). C: Spectral decomposition blend of three frequency magnitude volumes (red = 27 Hz, green = 33 Hz, blue = 57 Hz) draped on the LMM horizon, showing domal feature (A) located above V1, and frequency anomaly (B) located above V2 and V3. lobate flow feature interpreted to represent material extruded through the mud volcano. D: Perspective view of LMM horizon with draped spectral decomposition blend highlighting pipe located above domal feature (A), and frequency anomaly (B) above V2 and V3. E: Amplitude time slices at 0.1 s increments between 0.5 and 0.9 s TWT. Pipe is clearly visible within Upper Miocene carbonates on 0.5 and 0.6 s slices. Domal feature (A) and amplitude anomaly (B) are visible on 0.7 s slice, which corresponds to the approximately flat-lying LMM horizon. Polygonally faulted Lower Miocene claystone sequence (PFS) located beneath C and above the largest volcanic edifice (V1) is visible on 0.8 and 0.9 s slices.

Figure 6. Three-stage schematic model for burial of volcanic complex and subsequent influence on subsurface fluid flow.

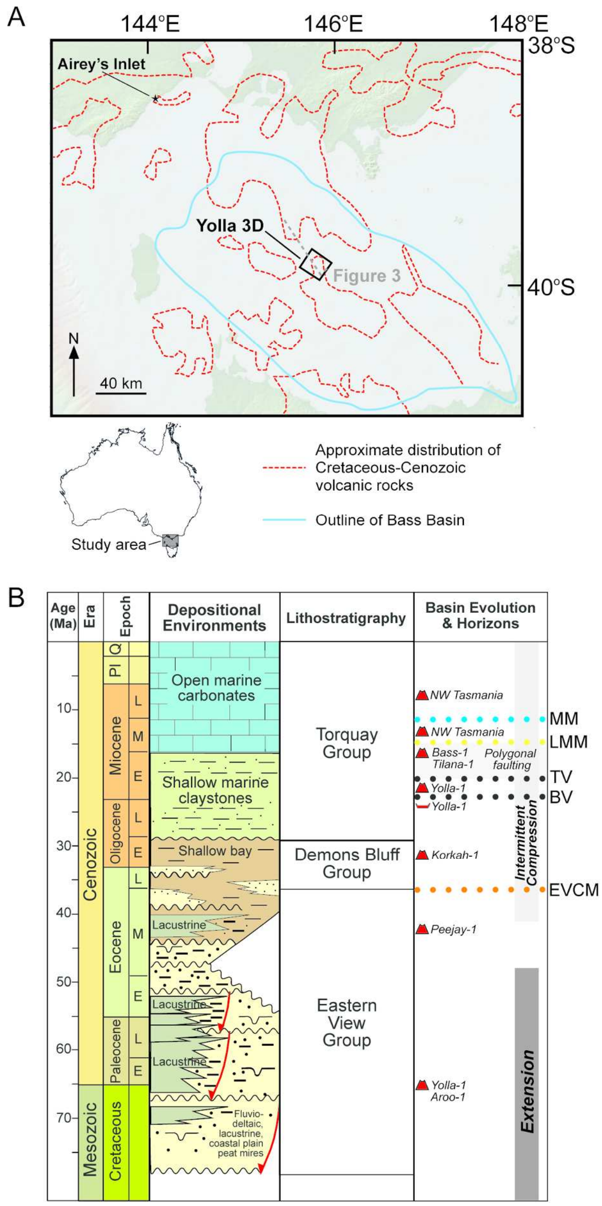

Figure 1. A: Location of Bass Basin, including approximate distribution of Cretaceous-Cenozoic age igneous rocks, location of the Yolla 3D seismic survey and the regional seismic profile shown in Figure 3. Inset map shows location of study area in relation to the Australian continent. B: Summary chart of Bass Basin stratigraphy, depositional environments, tectonic events, interpreted seismic horizons, and recorded episodes of extrusive and intrusive magmatism. Modified after Cummings et al. (2014), timing of deformation modified after Holford et al. (2014) and timing of magmatic events from Meeuws et al. (2016).

107x216mm (300 x 300 DPI)

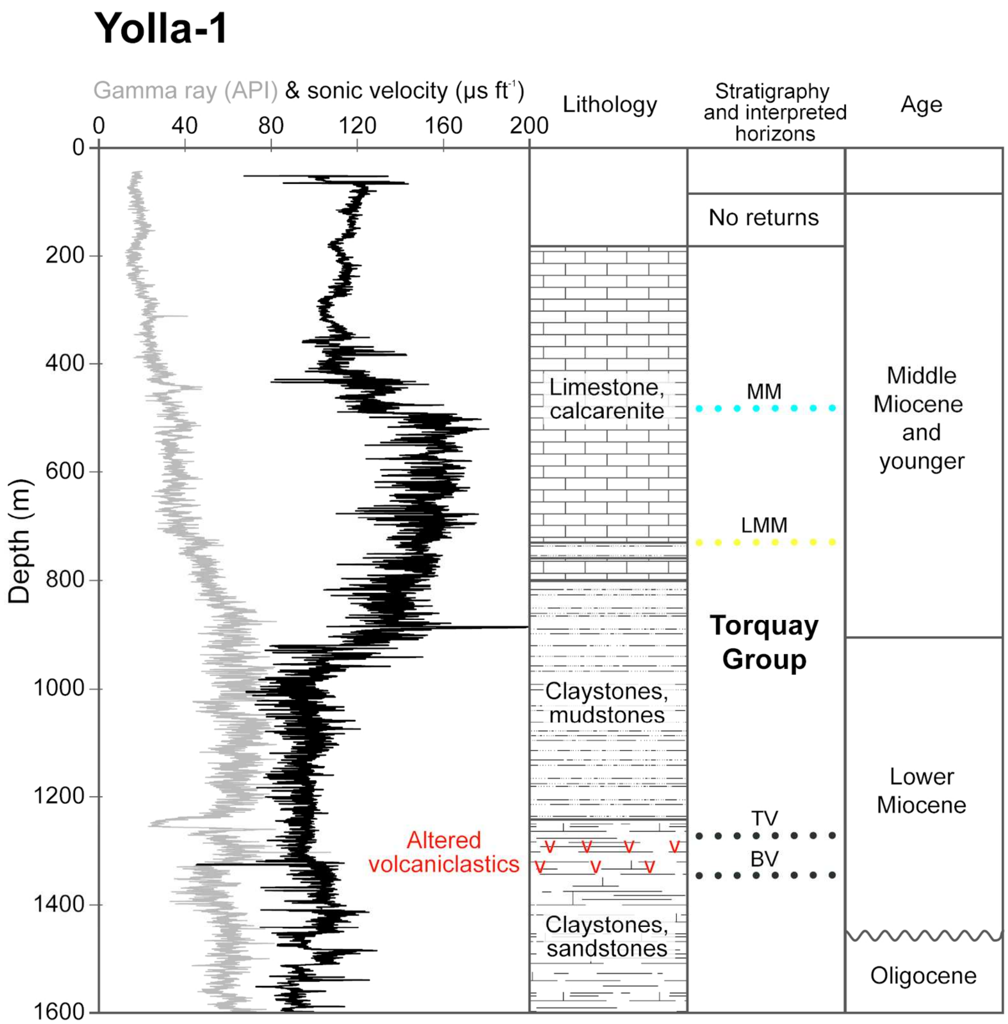

Lithologic, stratigraphic and sonic velocity and gamma ray log data for the shallowest 1600 m of rock section penetrated by the Yolla-1 well, showing the context of the interpreted horizons within the Torquay Group.

148x152mm (300 x 300 DPI)

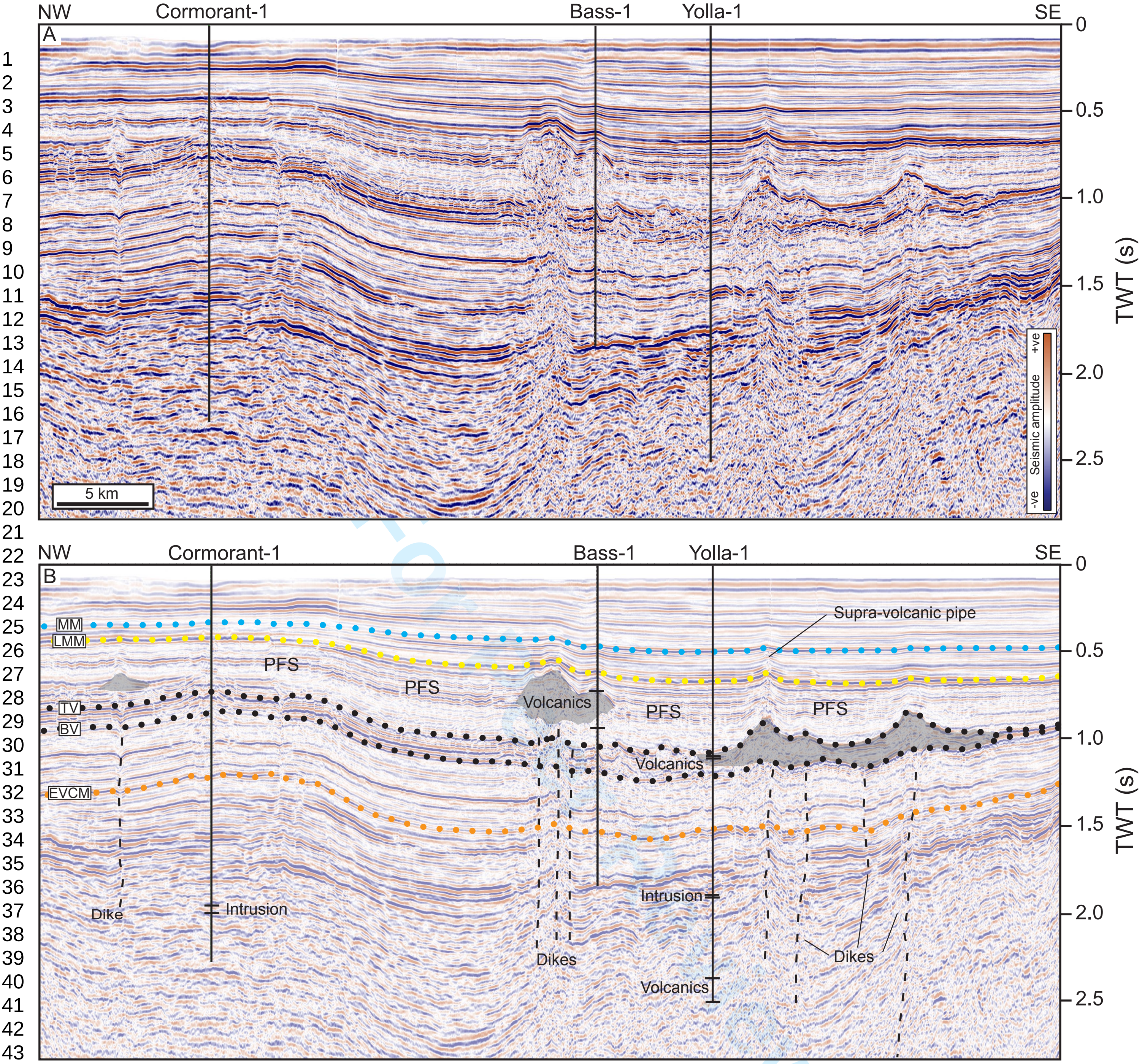
NW
Cormorant-1
Bass-1
Yolla-1
SE
A
0
0.5
1.0
1.5
2.0
2.5
TWT (s)
5 km
-ve
Seismic amplitude
+ve
B
MM
LMM
TV
BV
EVCM
PFS
Volcanics
Supra-volcanic pipe
Dike
Intrusion
Dikes

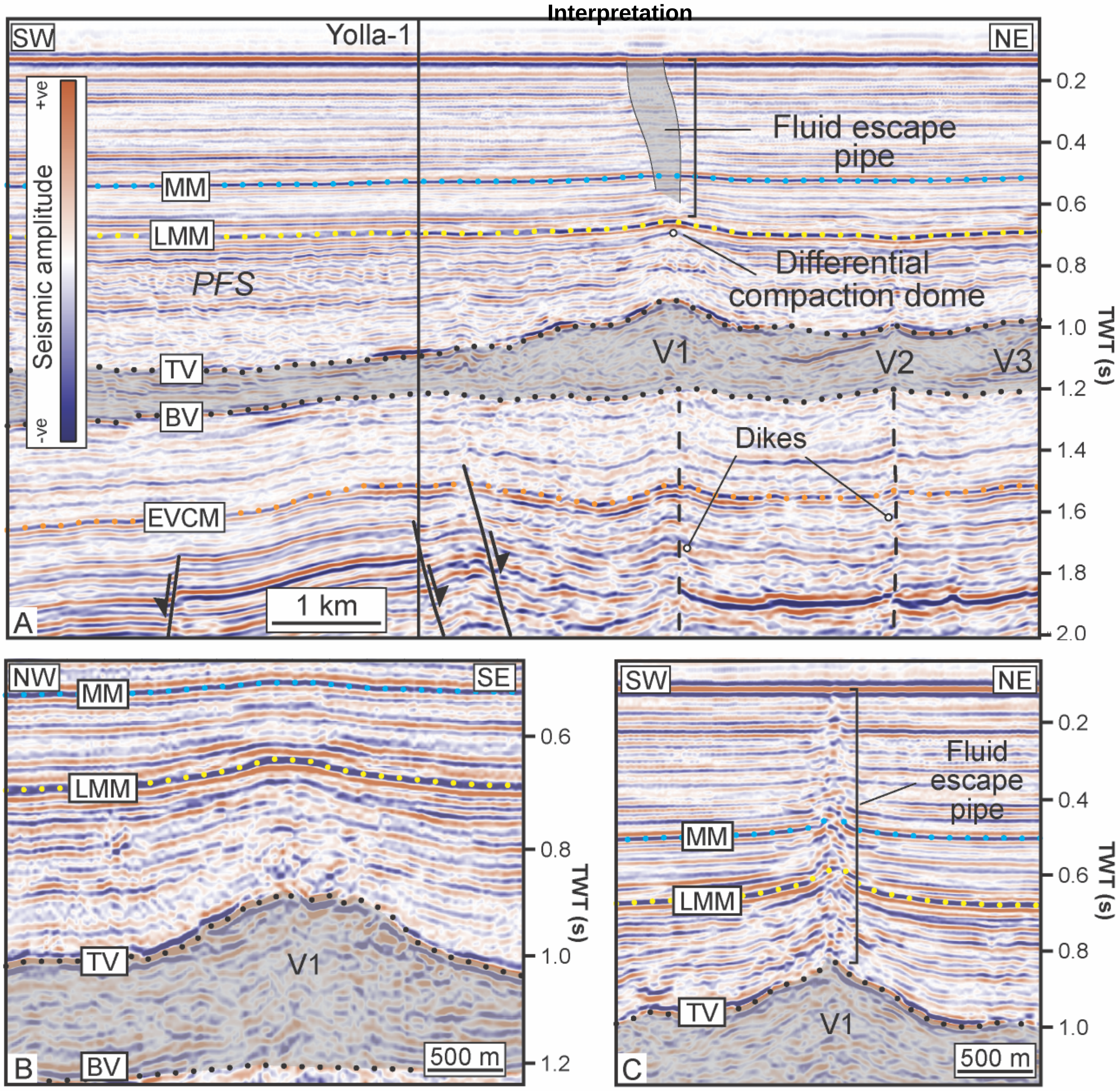
SW
Yolla-1
NE
Fluid escape pipe
MM
LMM
Differential compaction dome
PFS
Seismic amplitude
+ve
-ve
TV
V1
V2
V3
BV
Dikes
EVCM
1 km
A
0.2
0.4
0.6
0.8
1.0
1.2
1.4
1.6
1.8
2.0
TWT (s)
NW
SE
MM
LMM
TV
V1
BV
500 m
B
0.6
0.8
1.0
1.2
TWT (s)
SW
NE
Fluid escape pipe
MM
LMM
TV
V1
500 m
C
0.2
0.4
0.6
0.8
1.0
TWT (s)

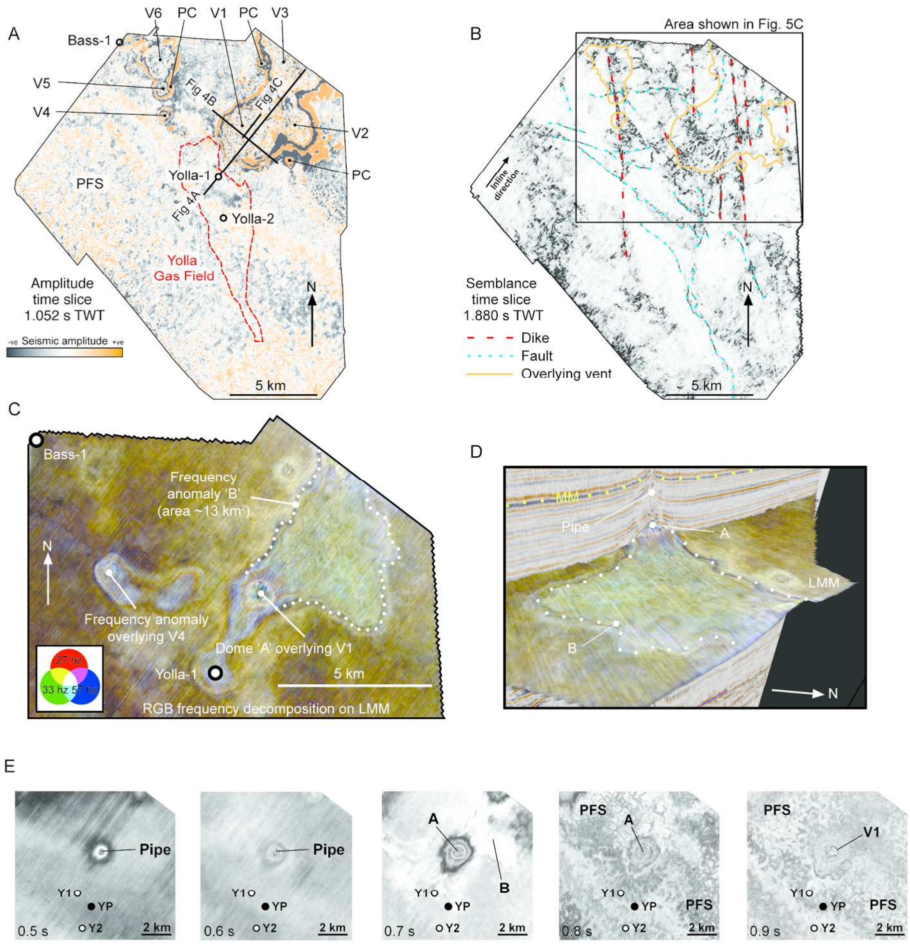

Figure 5. A: Seismic amplitude time slice (1.052 s TWT). Volcanic sequences are marked by high amplitude events that are easily distinguishable from surrounding sedimentary rocks. Gas-water contact of the Yolla hydrocarbon field is projected upwards onto this slice. Six main volcanoes (V1-V6) and a number of smaller parasitic cones (PC) are identified. B: Seismic semblance time slice (1.880 s TWT), highlighting discontinuities within the seismic volume (shown in black). Slice is annotated to distinguish between generally curvilinear faults (shown by blue dashed lines), interpreted dikes (shown by red dashed lines) and the outlines of overlying volcanoes (orange). C: Spectral decomposition blend of three frequency magnitude volumes (red = 27 Hz, green = 33 Hz, blue = 57 Hz) draped on the LMM horizon, showing domal feature (A) located above V1, and frequency anomaly (B) located above V2 and V3. lobate flow feature interpreted to represent material extruded through the mud volcano. D: Perspective view of LMM horizon with draped spectral decomposition blend highlighting pipe located above domal feature (A), and frequency anomaly (B) above V2 and V3. E: Amplitude time slices at 0.1 s increments between 0.5 and 0.9 s TWT. Pipe is clearly visible within Upper Miocene carbonates on 0.5 and 0.6 s slices. Domal feature (A) and amplitude anomaly (B) are visible on 0.7 s slice, which corresponds to the approximately flat-lying LMM horizon. Polygonally faulted Lower Miocene claystone sequence (PFS) located beneath C and above the largest volcanic edifice (V1) is visible on 0.8 and 0.9 s slices.

198x203mm (300 x 300 DPI)

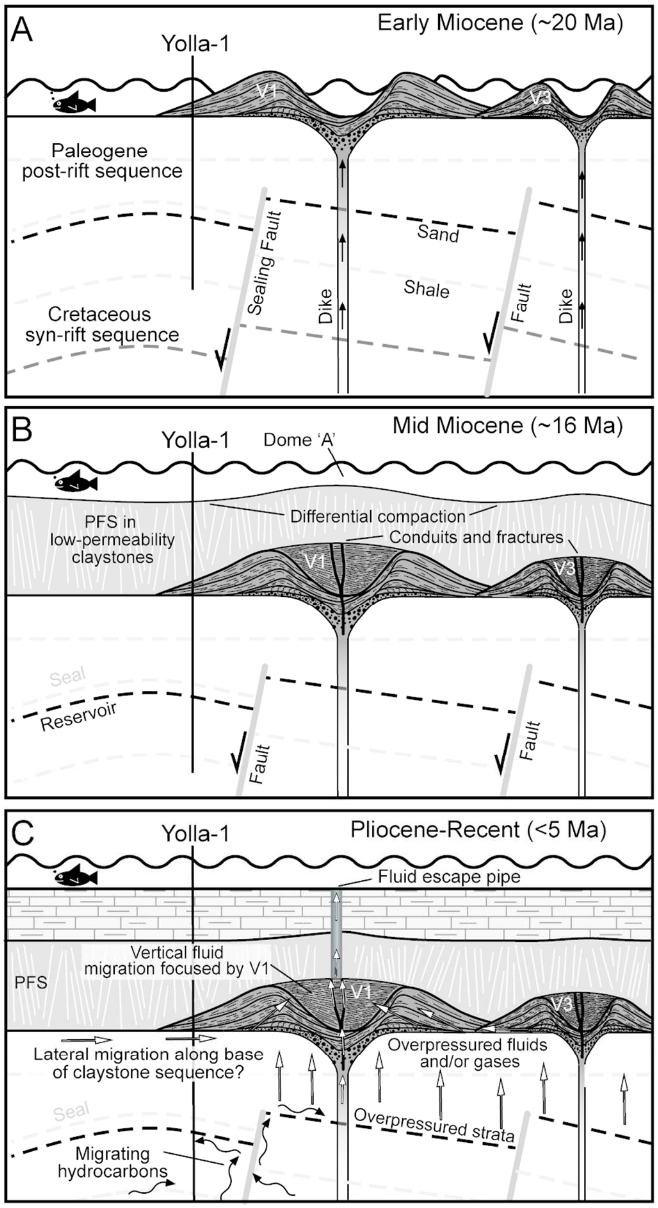

Figure 6. Three-stage schematic model for burial of volcanic complex and subsequent influence on subsurface fluid flow.

75x138mm (300 x 300 DPI)